

HOSTED BY



Contents lists available at ScienceDirect

Journal of King Saud University – Science

journal homepage: [www.sciencedirect.com](http://www.sciencedirect.com)

Original article

# Kinetics of the catalytic oxidation of toluene over Mn,Cu co-doped Fe<sub>2</sub>O<sub>3</sub>: Ex situ XANES and EXAFS studies to investigate mechanism



Van Dien Dang<sup>a,\*</sup>, Akhil Pradiprao Khedulkar<sup>b</sup>, Joemer Adorna Jr<sup>b</sup>, Van-Anh Thai<sup>c</sup>, Bidhan Pandit<sup>d,\*</sup>, Xuan-Hoan Nguyen<sup>a</sup>, Tan-Hiep Dang<sup>e</sup>, Lavish Kansal<sup>f</sup>, Niraj Kumar Jha<sup>g,\*</sup>, Mohd Ubaidullah<sup>h</sup>

<sup>a</sup> Faculty of Biology and Environment, Ho Chi Minh City University of Industry and Trade, 140 Le Trong Tan, Ho Chi Minh 700000, Viet Nam

<sup>b</sup> Department of Biomedical Engineering and Environmental Sciences, National Tsing Hua University, Hsinchu 30013, Taiwan

<sup>c</sup> Institute of Aquatic Science and Technology, National Kaohsiung University of Science and Technology, Kaohsiung City 81157, Taiwan

<sup>d</sup> Department of Materials Science and Engineering and Chemical Engineering, Universidad Carlos III de Madrid, Avenida de la Universidad 30, 28911 Leganés, Madrid, Spain

<sup>e</sup> Department of Chemical Engineering, Ho Chi Minh City University of Industry and Trade, 140 Le Trong Tan, Ho Chi Minh 700000, Viet Nam

<sup>f</sup> School of Electronics and Electrical Engineering, Lovely Professional University, Phagwara, India

<sup>g</sup> Department of Biotechnology, School of Engineering and Technology, Sharda University, Greater Noida 201310, India

<sup>h</sup> Department of Chemistry, College of Science, King Saud University, P.O. Box 2455, Riyadh 11451, Saudi Arabia

## ARTICLE INFO

### Article history:

Received 30 May 2023

Revised 17 July 2023

Accepted 19 July 2023

Available online 25 July 2023

### Keywords:

Catalytic oxidation

Toluene

Kinetics

Langmuir-Hinshelwood

Mars-van Krevelen

## ABSTRACT

In this study, the catalytic mechanism of Mn,Cu-Fe<sub>2</sub>O<sub>3</sub> catalyst was directly determined through reaction kinetics coupled with surface characterization. The impact of operating conditions on the catalytic performance of Mn,Cu-Fe<sub>2</sub>O<sub>3</sub> nanocomposite for toluene oxidation in a continuous fixed-bed reactor was investigated. It was found that Mn,Cu-Fe<sub>2</sub>O<sub>3</sub> catalyst gave the best catalytic performance in toluene removal when the initial concentrations of toluene and oxygen were at 165 ppmv and 10% at a flow rate of 200 mL min<sup>-1</sup>, respectively. Subsequently, Power-law, Mars-van Krevelen, and Langmuir-Hinshelwood models were developed to describe the kinetics of the total toluene oxidation for both toluene- and oxygen-dependent mixtures in a range of temperatures. According to the results, the basic Power-law model could not properly represent the kinetics of toluene oxidation over the catalyst. Meanwhile, the Mars-van Krevelen model allows for determining the kinetic mechanism under the variation of C<sub>7</sub>H<sub>8</sub> concentration. The Langmuir-Hinshelwood model is attainable to express the kinetics of the oxygen-involved reaction mechanism. Moreover, the change in the structure of Mn,Cu-Fe<sub>2</sub>O<sub>3</sub> catalyst after the catalytic reaction was characterized by X-ray Absorption Near-edge Structure (XANES) and Extended X-ray Absorption Fine Structure (EXAFS) measurements to confirm the catalytic mechanism determined through reaction kinetics. The achieved results suggest the possibility of using various models to justify the correlation between model-simulated and experimental data for VOCs oxidation in a continuous-flow catalytic reactor.

© 2023 The Authors. Published by Elsevier B.V. on behalf of King Saud University. This is an open access article under the CC BY-NC-ND license (<http://creativecommons.org/licenses/by-nc-nd/4.0/>).

## 1. Introduction

Volatile organic compounds (VOCs), known as carcinogenic pollutants, are released through various sources such as solvents,

fossil fuel thermal power plants, and transportation. They are precursors for the formation of photochemical smog and particulate matter, which threaten human health and the environment (Zhang et al., 2020). Although noble metals (Pt, Au, Pd) are highly active for catalytic oxidation of toluene and other VOCs oxidation, the high synthesizing cost and difficult regulation of particle size restrain their large-scale application (Zang et al., 2019). Hence, low-cost transition metal oxides-based (i.e., Mn, Cu, Ce, Ti, Co) catalysts are recognized as alternative materials because of their high activity and poisoning counteraction (Figueredo et al., 2020; Li et al., 2021). In addition to the catalyst composition, kinetic model derivation, which makes it possible to foresee the reaction rate of VOCs combustion over the catalyst, is another factor that must be considered for the catalytic combustion technique. Various

\* Corresponding authors.

E-mail addresses: [diendv@hufi.edu.vn](mailto:diendv@hufi.edu.vn) (V.D. Dang), [bpandit@ing.uc3m.es](mailto:bpandit@ing.uc3m.es) (B. Pandit), [niraj.jha@sharda.ac.in](mailto:niraj.jha@sharda.ac.in) (N.K. Jha).

Peer review under responsibility of King Saud University.



Production and hosting by Elsevier

<https://doi.org/10.1016/j.jksus.2023.102812>

1018-3647/© 2023 The Authors. Published by Elsevier B.V. on behalf of King Saud University.

This is an open access article under the CC BY-NC-ND license (<http://creativecommons.org/licenses/by-nc-nd/4.0/>).

conceptual models defining the surface mechanism were theorized in the quest to construct reliable kinetic models for the catalytic oxidation processes (Mohammed et al., 2020; Xu et al., 2023).

Moreover, it may be hard to explain the catalytic mechanism of the as-prepared material under reaction conditions, especially in the existence of various reactants and their interaction with the catalyst's surface (He et al., 2020; Lin et al., 2023). To our best knowledge, current kinetic expression is not available for describing the oxidation route as well as the catalytic mechanism. Therefore, constructing suitable kinetic models to contrast the experimental data of the oxidation pathway is needed to support the catalytic mechanism. Accordingly, kinetic modeling can provide a detailed understanding of the oxidation reaction rate and the effect of contaminant and oxygen feed on a catalytic process (Shakor et al., 2022). Several studies on the kinetic models have been carried out to hypothesize different conceptual approaches for describing the catalyst surface mechanism in the catalytic oxidation of VOCs (Hu, 2011; Zou et al., 2019). Power-law (P-L) model is the most facile mathematical kinetic equation used to express the relationship between the reaction rate with the rate constant and reactant concentration or pressure (Tseng and Chu, 2001). Mars-Van Krevelen (MVK) and Langmuir-Hinshelwood (L-H) models are used to express the reaction rate, as well as to elucidate the mechanism of catalytic oxidation of VOCs over metal oxides (Arzamendi et al., 2009). The MVK model usually illustrates the acute and absolute reactions over the metal oxides-derived catalysts (Genty et al., 2019; Vannice, 2007). Experimental data from kinetics of methane in the oxygen-rich mixtures via cobalt oxide (Bahlawane, 2006); the oxidation of VOCs over  $\text{SmMnO}_3$  perovskites (Liu et al., 2019), and the oxidation of toluene over  $\text{CoAlCe}$  catalyst (Genty et al., 2019) were all well expressed by the MVK model. L-H model, on the other hand, is used to investigate the adsorption and desorption of gas molecules, which interact with reactants on the catalyst surface (Mahmood et al., 2021). The L-H model is also used to explain the dependence of oxidation rate on reactant concentration in heterogeneous catalytic processes (Dang et al., 2021; Wang et al., 2002). Since the catalytic reaction is a chemical adsorption, L-H model shows more consistent with the catalytic oxidation of styrene by  $\text{Fe}_2\text{O}_3/\text{MnO}$  (Tseng and Chu, 2001) than that of the MVK model. The most challenging data to derive in a catalytic oxidation system is involved kinetic parameters.

The XANES method in XAS (X-ray Absorption Spectroscopy) is often used to specify the oxidation state and association status of materials because of its sensitivity to the elements valence state (Cai et al., 2019). Besides, by using XANES, it is able to distinguish the species of identical standard oxidation stages but distinctive coordination due to its sensitivity to bondings and oxidation states. In this study, XANES was utilized to analyze the difference in metal valence before and after the reaction. Accordingly, the change in the structure before and after the reaction is based on the valence alteration of metal elements (Fe, Mn, and Cu) and the difference in the atomic structure of the second layer from the absorbing atoms. Hence, the intermediate product of the catalyst surface in the catalytic reaction can be determined. Moreover, the EXAFS provides information about the structure and bonding of an excited atom's local environment, including the identity of distance and the number of adjacent atoms and the disorder grade in a specific atomic shell (Teo and Exafs, 2012). Theoretically, the catalyst does not participate in the reaction, but practically, the structure of the catalyst can be influenced by surface reactions, reactants, and residues. Hence, EXAFS can provide more accurate differences in the structure before and after the catalytic reaction (Zhao et al., 2015).

In this study, we synthesized Mn,Cu co-doped  $\text{Fe}_2\text{O}_3$  (hereafter denoted as Mn,Cu- $\text{Fe}_2\text{O}_3$ ), calcined at 400 °C for toluene oxidation in a continuous fixed-bed reactor. The obtained experimental

results provide preliminary data to evaluate the aforementioned kinetic models for the best representative of the complete toluene oxidation reactions over Mn,Cu- $\text{Fe}_2\text{O}_3$  catalyst. Particularly, kinetic models are first built up by considering the nature of oxidation reactions on active sites, then their applicability are justified by comparing the as-simulated model fittings with experimental data. Subsequently, the obtained kinetics and the intrinsic structure characterization of Mn,Cu- $\text{Fe}_2\text{O}_3$  catalyst after reaction is the premise to confirm a catalytic mechanism.

## 2. Experimental

### 2.1. Synthesis of catalyst

The iron manganese copper oxide Mn,Cu- $\text{Fe}_2\text{O}_3$  was synthesized by co-precipitation method followed by pyrolysis. Typically, 3 mol  $\text{Fe}(\text{NO}_3)_3$ , 1 mol  $\text{Mn}(\text{NO}_3)_2$ , and 1 mol  $\text{Cu}(\text{NO}_3)_2$  (Sigma-Aldrich, >99%) were dissolved in a beaker containing 0.5 L of DI water under well mixing, so-called solution A. In another beaker (B), 0.25 mol  $\text{Na}_2\text{CO}_3$  (Fluka, USA) was dissolved in 0.5 L of DI water to make another solution (B). The solution in beaker A was gradually added to the solution in beaker B under the well-mixing condition to get a homogeneous solution, which was then kept standstill for 24 h. The precipitation was collected, washed and dried at 105 °C for 12 h. The obtained powder was ground and annealed in air at 400 °C for 4 h. After cooling down, the final product was collected and stored in a closed container.

### 2.2. Characterization

The change in structural properties of the as-prepared catalyst after oxidation process was investigated via several measurements. The specific atoms of the as-prepared material were detected using X-ray Absorption Near-edge Structure (XANES) measurement. The structure of the region close to central atom was determined by and Extended X-ray Absorption Fine Structure (EXAFS) characterization. Both XANES and EXAFS measurements were performed in National Synchrotron Radiation Research Center, Hsinchu city, Taiwan. All samples were characterized by K-edge XANES and EXAFS in transmission mode under normal conditions using Fe, Mn, and Cu foil as references.

### 2.3. Catalytic experiments

Catalytic oxidation of toluene over Mn,Cu- $\text{Fe}_2\text{O}_3$  was carried out in a continuous-flow fixed-bed system. The reactor made of glass tube with 9.5 cm long and inner diameter of 2 cm was loaded with 48 g of quartz (1 mm diameter) coated by 0.2 g of catalyst. The gaseous mixture was made up of  $\text{N}_2$ ,  $\text{O}_2$ , and toluene in synthetic air by adjusting the flow rate from three sets of these corresponded gas cylinders to have different  $\text{C}_7\text{H}_8$  and  $\text{O}_2$  concentrations. The reactor was wrapped around and heated by a heating tape (300 W). The temperature of reactor was monitored by a thermocouple and controlled in the range of 220–320 °C. The toluene conversion efficiency was measured by a gas chromatograph (GC, PerkinElmer Clarus 500 GC, FID). A blank experiment was implemented without catalyst coated on quartz sands using the same feed stream to assess the effect of temperature on the catalytic activity.

### 2.4. Optimization of operating parameters for $\text{C}_7\text{H}_8$ conversion

To understand the effect of operating variables on  $\text{C}_7\text{H}_8$  oxidation efficiency over Mn,Cu- $\text{Fe}_2\text{O}_3$ , the system was proceeded non-isothermally under different initial concentrations of  $\text{C}_7\text{H}_8$  and

O<sub>2</sub>, and at different flow rates in the feed stream. The effect of initial concentration of C<sub>7</sub>H<sub>8</sub> was tested by varying C<sub>7</sub>H<sub>8</sub> concentration from 55 to 220 ppmv, while keeping the concentration of oxygen and flow rate (Q) constant (C<sub>O<sub>2</sub></sub> = 10%, Q = 200 mL min<sup>-1</sup>). The effect of oxygen concentration in the feed stream was evaluated by maintaining the concentration of C<sub>7</sub>H<sub>8</sub> and flow rate constant (C<sub>C<sub>7</sub>H<sub>8</sub></sub> = 165 ppmv, Q = 200 mL min<sup>-1</sup>), but altering the oxygen concentration of oxygen in the range of 1–30%. The influence of flow rate (from 200 to 500 mL min<sup>-1</sup>) on the catalytic performance was evaluated at constant O<sub>2</sub>/C<sub>7</sub>H<sub>8</sub> ratio (10<sup>4</sup>: 165 = 61). O<sub>2</sub> was used as an oxidizing agent, and the mass of catalyst in the reactor was maintained stable for all experiments.

The catalytic experiment was conducted at different temperatures (202–307 °C) for testing the mass balance. During the experiment, C<sub>7</sub>H<sub>8</sub> concentration, O<sub>2</sub> concentration, and flow rate are adjusted to 165 ppmv, 10%, and 200 mL min<sup>-1</sup>, respectively. The conversion rate of CO<sub>2</sub> was considered as a function of the conversion rate of C<sub>7</sub>H<sub>8</sub>. The inlet concentration of C<sub>7</sub>H<sub>8</sub> was controlled, while the outlet concentrations of C<sub>7</sub>H<sub>8</sub> and CO<sub>2</sub> were analyzed for mass balance calculation, which is the base to determine experimental reaction rate.

## 2.5. Kinetic modelling

The catalytic reaction is expressed by the function of conversion rate (Y-axis) versus the temperature (X-axis). Generally, the conversion rate is enhanced with an increase in temperature. In a catalytic reaction dynamic experiment, different concentrations of a reactant results in different reaction rates. Therefore, the reaction rate is discussed according to each catalytic reaction mode using MVK, and L-H models. From the linearity fitting of each temperature, the reaction rate constant (k) is then derived and used for linearity regression to find the activation energy using the Arrhenius equation.

The reaction rate (–r) can be calculated as:

$$-r = \frac{F_e}{V} W = \frac{F_e}{V} \left( \frac{C_{in} - C_{out}}{C_{in}} \right) \quad (1)$$

where F<sub>e</sub> is reactant flow rate (mol s<sup>-1</sup>), V is reactor volume (cm<sup>3</sup>), W is conversion rate ( $W = \frac{C_{in} - C_{out}}{C_{in}} \times 100\%$ ), C<sub>in</sub> and C<sub>out</sub> are the influent and effluent concentrations of reactant, respectively.

### 2.5.1. Power-law model

The oxidation rate as a function of toluene and oxygen concentration is described via the Power-law model:

$$-r = \frac{dC}{dt} = k C_e^n C_{O_2}^m \quad (2)$$

where r is reaction rate of toluene (mol cm<sup>-3</sup> s<sup>-1</sup>), k is rate constant (s<sup>-1</sup>), C<sub>e</sub>, C<sub>O<sub>2</sub></sub> are concentrations of toluene and oxygen, respectively (mol cm<sup>-3</sup>), n and m are reaction orders.

Because C<sub>O<sub>2</sub></sub> >> C<sub>e</sub>, hence C<sub>O<sub>2</sub></sub> can be assumed to be a constant, the equation can be rewritten as follows:

$$\ln(-r) = \ln(k_p) + m \times \ln(C_e) \quad (3)$$

where k<sub>p</sub> is the rate constant in the case of C<sub>O<sub>2</sub></sub> >> C<sub>e</sub>.

When concentration of O<sub>2</sub> is fixed, the reaction rate of toluene catalytic oxidation is calculated by linear regression fitting. The slope m represents reaction order, whereas rate constant k<sub>p</sub> can be derived from the intercept ln(k<sub>p</sub>) at each heating temperature point.

### 2.5.2. Mars-van Krevelen model

MVK model consists of two steps. The first is the reaction of oxidized catalyst sites (OCS) and toluene to form reduced catalyst

sites (RCS). Another is the reaction of RCS and O<sub>2</sub> from the gas phase to regenerate OCS for the next cycle. The process can be elucidated by the following reaction equations:



When the combustion reaction of toluene reaches equilibrium, 1 mol of toluene needs 3 mol of oxygen to be completely oxidized (C<sub>7</sub>H<sub>8</sub> + 3O<sub>2</sub> → 2CO<sub>2</sub> + 2H<sub>2</sub>O), the reaction rate (r) can be combined into the following formula:

$$-r = \frac{k_e C_e k_{O_2} C_{O_2}}{3k_e C_e + k_{O_2} C_{O_2}} \quad (6)$$

where k<sub>O<sub>2</sub></sub> (mol cm<sup>-3</sup> s<sup>-1</sup>) is reaction rate constant depending on the oxygen concentration, k<sub>e</sub> (mol cm<sup>-3</sup> s<sup>-1</sup>) is reaction rate constants depending on the toluene concentration. Eq. (6) can be altered:

$$\frac{1}{-r} = \frac{3}{k_{O_2} C_{O_2}} + \frac{1}{k_e C_e} \quad (7)$$

Since C<sub>O<sub>2</sub></sub> is a constant, k<sub>e</sub> and k<sub>O<sub>2</sub></sub> can be derived from the slope of a linear regression fitting (1/(–r) versus 1/C<sub>e</sub>) for each temperature point.

### 2.5.3. Langmuir – Hinshelwood model

In Langmuir Hinshelwood model, it is assumed that all catalyst components have the same activation position, where oxygen and reactant molecules are adsorbed (hereafter denoted by C<sub>7</sub>H<sub>8</sub><sup>\*</sup>, O<sup>\*</sup>, and O<sub>2</sub><sup>\*</sup>), then the reactions take place as follows:



Oxygen molecule adsorption and oxygen atom adsorption are explained separately:

(1) Reactions involving the adsorption of molecular oxygen:

$$-r = k\varphi_e \varphi_{O_2} = \frac{kK_e C_e K_{O_2} C_{O_2}}{(1 + K_e C_e + K_{O_2} C_{O_2})^2} \quad (11)$$

where φ<sub>e</sub> and φ<sub>O<sub>2</sub></sub> represent the adsorbed sites ratio for toluene and O<sub>2</sub>, respectively; K<sub>e</sub> and K<sub>O<sub>2</sub></sub> represent the equilibrium adsorption constant for C<sub>7</sub>H<sub>8</sub> and O<sub>2</sub>, respectively.

(2) Reactions involving the adsorption of atomic oxygen:

$$-r = k\varphi_e \sqrt{\varphi_{O_2}} = \frac{kK_e C_e \sqrt{K_{O_2} C_{O_2}}}{(1 + K_e C_e + \sqrt{K_{O_2} C_{O_2}})^2} \quad (12)$$

where k, K<sub>e</sub>, and K<sub>O<sub>2</sub></sub> are constants at the same operating temperature. Eq. (12) can be simplified to:

$$\sqrt{\frac{C_e}{-r}} = \frac{1}{\sqrt{K'}} + \frac{K''}{\sqrt{K'}} C_e \quad (13)$$

where  $K' = \frac{kK_e K_{O_2} C_{O_2}}{(1 + K_{O_2} C_{O_2})^2}$ ,  $K'' = \frac{K_e}{1 + K_{O_2} C_{O_2}}$

When the concentration of toluene is fixed, the Eq. (13) is simplified into two linear equations:

a. Molecular oxygen (O<sub>2</sub>) adsorption:

$$\sqrt{\frac{C_{O_2}}{-r}} = \frac{1}{\sqrt{K'_1}} + \frac{K''_1 C_{O_2}}{\sqrt{K'_1}} \quad (14)$$

$$K'_1 = \frac{kK_e C_e K_{O_2}}{(1 + K_e C_e)^2} K''_1 = \frac{K_{O_2}}{1 + K_e C_e}$$

A plot of  $\sqrt{\frac{C_{O_2}}{-r}}$  versus  $C_{O_2}$  provides a linear regression.

b. Atomic oxygen (O) adsorption:

$$\sqrt{\frac{C_{O_2}}{-r}} = \frac{1}{\sqrt{K'_2}} + \frac{K''_2 \sqrt{C_{O_2}}}{\sqrt{K'_2}} \quad (15)$$

$$\text{where } K'_2 = \frac{kK_e C_e \sqrt{K_{O_2}}}{(1 + K_e C_e)^2}, K''_2 = \frac{\sqrt{K_{O_2}}}{1 + K_e C_e}$$

A plot of  $\sqrt{\frac{C_{O_2}}{-r}}$  versus  $\sqrt{C_{O_2}}$  provides a linear regression.

#### 2.5.4. Activation energy

The activation energy ( $E_a$ ,  $\text{kJ mol}^{-1}$ ) was calculated using Arrhenius equation:

$$\ln k = \ln A - \frac{E_a}{RT} \quad (16)$$

where  $k$  is rate constant ( $\text{s}^{-1}$ ),  $A$  is frequency factor ( $\text{s}^{-1}$ ),  $T$  is operating temperature (K), and  $R$  is ideal gas constant ( $8.31 \times 10^{-3} \text{ kJ mol}^{-1} \text{ K}^{-1}$ ).

## 3. Results and discussion

### 3.1. Effects of operating parameters

#### 3.1.1. Initial concentration of toluene

It is well-known that the operating conditions for catalytic oxidation are changeable and complicated. Hence, exploring the effects of working conditions on toluene conversion is essential to get the highest conversion efficiency of the Mn,Cu-Fe<sub>2</sub>O<sub>3</sub> catalyst in practical application. Fig. 1a displays the dependence of conversion rate on the initial concentration of toluene at a constant O<sub>2</sub> concentration (10%) and inlet flow rate (200 L min<sup>-1</sup>). The conversion rate decreases when the concentration of toluene increases from 55 to 220 ppmv. Specifically, when the heating temperature is in the range of 200–270 °C, the conversion rate is inversely proportional to the concentration of feeding toluene, i.e., the higher the concentration of toluene is, the lower the conversion rate will be (Fig. S1a). This result may be due to the limit of the active surface of Mn,Cu-Fe<sub>2</sub>O<sub>3</sub> catalyst for toluene adsorption before oxidation. Because the reactor is a continuous flow, toluene molecules probably compete with each other for the adsorption on Mn,Cu-Fe<sub>2</sub>O<sub>3</sub> catalyst surface. In other words, the more C<sub>7</sub>H<sub>8</sub> molecules enter the reactor, the higher competition for them to occupy on the catalyst surface, resulting in more C<sub>7</sub>H<sub>8</sub> molecules to be kicked out. Hence, it is concluded that the reactant adsorption over the catalyst surface is a rate-determining stage.

It is noteworthy that heating temperature has a supportive effect on the efficiency of C<sub>7</sub>H<sub>8</sub> conversion. Remarkably, at 220 °C, the conversion rate of four investigated C<sub>7</sub>H<sub>8</sub> concentrations is under 20%. However, when the reactor temperature increases to 270 °C, the conversion rate of C<sub>7</sub>H<sub>8</sub> at 55, 110, 165, and 220 ppmv is 97, 95, 90, and 80%, respectively. At 290 °C, C<sub>7</sub>H<sub>8</sub> was removed nearly completely at most concentrations. When the heating temperature reaches 300 °C, C<sub>7</sub>H<sub>8</sub> was converted completely, which promotes the mass transfer process (Wu et al., 2021).

#### 3.1.2. Inlet concentration of O<sub>2</sub>

In terms of reactants, oxygen concentration also plays an indispensable role in the heterogeneous reaction of catalytic system. As illustrated in Fig. 1b, the conversion rate increases significantly when O<sub>2</sub> concentration is in the range of 1–5%, but varies slightly when O<sub>2</sub> concentration is in the range of 5–30%. Apparently, reaction rate changes obviously when oxygen concentration is within 5% but keeps constant when oxygen concentration is in the range of 5–30%. This result suggests that to achieve complete C<sub>7</sub>H<sub>8</sub> oxidation, the inlet O<sub>2</sub> should be maintained at a concentration greater than 5% (Fig. S1b).

When the O<sub>2</sub> concentration increase from 1 to 5%, the probability of oxygen adsorption on the metal oxide surface increases to replenish the oxygen vacancies made by consumed lattice oxygen, resulting in enhancement of C<sub>7</sub>H<sub>8</sub> oxidation (Hu, 2011). Therefore, once oxygen is supplied with a higher concentration, the oxidation will be accelerated. Previous studies also pointed out that metal oxides still can catalyze the oxidation of C<sub>7</sub>H<sub>8</sub> at low concentration or even without oxygen, which is assigned to the effect of lattice oxygen or OH groups on the catalyst surface (Su et al., 2020; Halim et al., 2007). When the supplied O<sub>2</sub> concentration is over 5%, the catalytic oxidation of toluene reaches a certain limit and no longer increases, leading to the unchanged performance of toluene oxidation.

The relationship between reaction rate and reactant concentration is shown in Table S1. Typically, the reaction rate increases when the concentration of O<sub>2</sub> and C<sub>7</sub>H<sub>8</sub> increases. According to the principle of L-H model, when the C<sub>7</sub>H<sub>8</sub> and O<sub>2</sub> are supplied to reactor with low level, increasing the concentration of C<sub>7</sub>H<sub>8</sub> and O<sub>2</sub> will also increase the reaction rate. This phenomenon takes place if the adsorption positions of reactants are different, the reaction rate will increase. In contrast, the same adsorption positions may lead to competitive adsorption among reactants, resulting in the reduction of the reaction rate. In terms of the MVK model, increasing O<sub>2</sub> concentration improves the reaction rate because more activation sites with oxygen vacancies are supplied on the metal oxide surface for toluene coupling and oxidation (Zhao et al., 2019).

#### 3.1.3. Flow rate

The change in the catalytic reaction efficiency under different flow rates was tested at different temperatures, while the ratio between C<sub>7</sub>H<sub>8</sub> and O<sub>2</sub> were kept constant. Fig. 1c shows that the reaction efficiency decreases when the flow rate increases. This result can be assigned to the overload of limited active catalyst surface due to the higher content of toluene in the reactor caused by the higher flow rate. Obviously, the catalytic oxidation of toluene over Mn,Cu-Fe<sub>2</sub>O<sub>3</sub> is the surface-supported reaction. Hence, the limited surface of Mn,Cu-Fe<sub>2</sub>O<sub>3</sub> catalyst cannot accommodate all toluene to be adsorbed on the Mn,Cu-Fe<sub>2</sub>O<sub>3</sub> catalyst surface, resulting in efficiency decrease. Moreover, at the flow rate of 200, 300, 400, and 500 mL min<sup>-1</sup>, the empty-bed residence time (EBRT), a fraction of catalyst volume (12 cm<sup>3</sup>) and flow rate (cm<sup>3</sup>/min), is calculated as 3.6, 2.4, 1.8, and 1.4 s, respectively. Decreasing EBRT from 3.6 s to 2.4 s caused a decrease in toluene removal efficiency by 13.2%, demonstrating that shorter residence time is not favorable for toluene to be adsorbed and decomposed on the Mn,Cu-Fe<sub>2</sub>O<sub>3</sub> catalyst surface, thereby reducing the reaction efficiency (Brandt et al., 2016). In overall, it is concluded that flow rate is conversely proportional to the conversion rate.

#### 3.1.4. Mass balance

In order to determine the catalytic oxidation conversion of toluene over Mn,Cu-Fe<sub>2</sub>O<sub>3</sub> catalyst in the reaction process, the change in concentration of both toluene and CO<sub>2</sub> was measured simultaneously through GC/FID. A converting system was used to

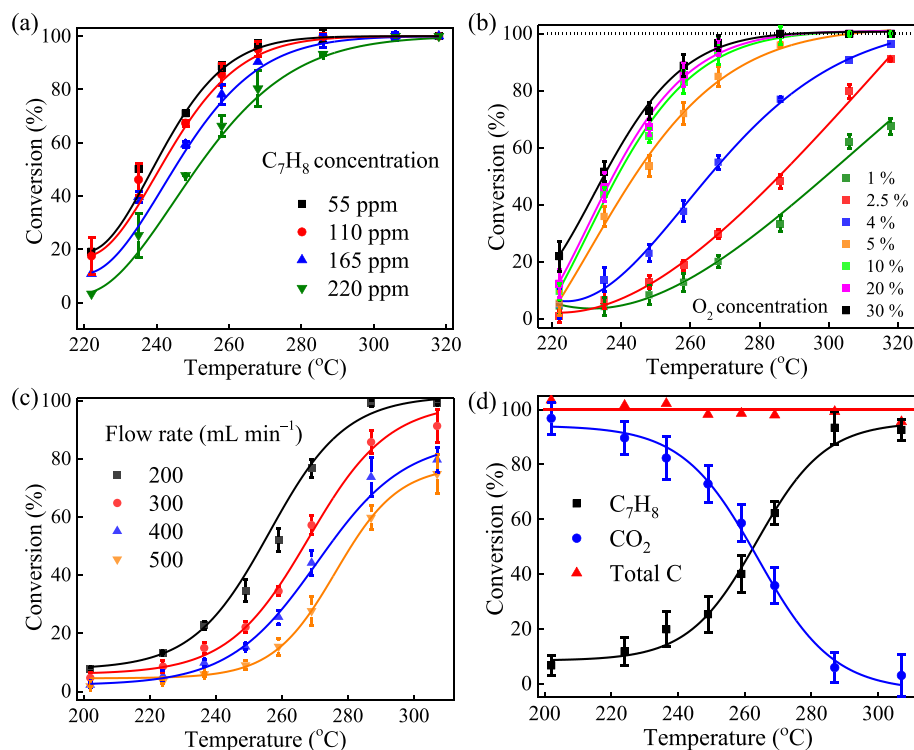


**Fig. 1.** (a) and (b) the effect of initial toluene concentration ( $C_{O_2} = 10\%$ ,  $Q = 200 \text{ mL min}^{-1}$ ) and inlet  $O_2$  concentration ( $C_{C_7H_8} = 165 \text{ ppmv}$ ,  $Q = 200 \text{ mL min}^{-1}$ ) on the conversion rate at different temperatures, respectively; (c) the effect of flow rate on catalytic activity ( $C_{O_2}/C_{C_7H_8}$  ratio = 91); (d) mass balance of  $C_7H_8$  and  $CO_2$  ( $C_{C_7H_8} = 165 \text{ ppmv}$ ,  $C_{O_2} = 10\%$ ,  $Q = 200 \text{ mL min}^{-1}$ ).

confirm if other intermediates are generated during the catalytic reaction. As presented in Fig. 1d, toluene is totally converted to  $CO_2$  without the generation of any intermediate products. Furthermore, the concentration of  $C_7H_8$  and  $CO_2$  are divided by the total carbon content (summary of  $C_7H_8$  and  $CO_2$ ) to find the individual conversion rate. Fig. S2 illustrates that the conversion of  $C_7H_8$  and production of  $CO_2$  approximately intersects at 50%, indicating that  $C_7H_8$  is completely oxidized to  $CO_2$ . Therefore, the relationship between the reactant ( $C_7H_8$ ) and product ( $CO_2$ ) suggests that the possible steps affecting the reaction rate are in the following order:  $C_7H_8$  adsorption,  $O_2$  adsorption,  $C_7H_8$  oxidation reaction, and product desorption.

### 3.2. Kinetic modelling

The process to carry out the modeling can be separated into two cases depending on the alteration of  $C_7H_8$  and  $O_2$  concentrations. In the first case, the initial concentration of  $C_7H_8$  is changed while the concentration of oxygen and flow rate are kept constant, the reaction rate at each investigated temperature point can be obtained using Eq. (1). The results are substituted to Eq. (3) for P-L model, substituted to Eq. (7) to derive reaction orders and reaction rate constants for MVK ( $k_e$ ) models, and substituted to Eq. (13) to get mixed rate constant  $K'$  and  $K''$  for L-H model. Subsequently, by using the Arrhenius equation (Eq. (16)), the activation energy ( $E_a$ ) can be determined. In the second case, the inlet oxygen concentration is changed while the concentration of toluene and flow rate are kept constant, the reaction rate at investigated temperature points can be obtained using Eq. (1). After that, the results are substituted to Eqs. 17 and 18 to get the reaction rate constants ( $K_1$ ,  $K_1'$ ) and ( $K_2$ ,  $K_2'$ ) for L-H models, respectively. From the linear plot of Arrhenius equation, the activation energy can be obtained using the reaction rate constants ( $K_1$ ,  $K_1'$ ) and ( $K_2$ ,  $K_2'$ ) against different

temperatures ( $1000/T$ ). The pairs ( $K_1$ ,  $K_1'$ ) and ( $K_2$ ,  $K_2'$ ) are used to calculate  $k$ ,  $K_e$ , and  $K_{O_2}$  for a reaction involving  $O_2$  and  $O$  adsorption, respectively. The best fit giving model can be specified based on determination coefficient ( $R^2$ ) and their activation energies.

#### 3.2.1. Power-law model

As displayed in Table S2, under constant oxygen concentration (10%), the reaction rate of toluene oxidation over  $Mn,Cu-Fe_2O_3$  catalyst increases as the reaction temperature increases. The linear regression fittings for the P-L model are shown in Fig. 2a, in which the slope represents the reaction order, whereas the intercepts symbolize the rate constant  $k_p$ . The Arrhenius fitting graph is exhibited in Fig. 2b with  $R^2 = 0.943$ . The activation energy is calculated to be  $164.8 \text{ kJ mol}^{-1}$ , and the frequency factor is  $11.1 \times 10^{12} \text{ s}^{-1}$ . Since the  $R^2$  value is low, the PL model is not suggested to be feasible for the catalytic oxidation of  $C_7H_8$  over  $Mn,Cu-Fe_2O_3$  catalyst. In general, the Power-law model mainly assumes a heterogeneous catalytic reaction mode based on homogeneous mode (Pandhare et al., 2018). Therefore, it is less applicable when complex reactions, such as adsorption or multi-molecular reactions, are involved. According to the catalytic reaction data results, the low catalytic reaction is more complicated and may include the mechanism of the reactant or product adsorption.

#### 3.2.2. Mars-van Krevelen model

Generally, the mechanism of MVK is explained that the adsorption of one molecule occurs on top of the previous adsorbed one. Specifically, MVK model clarifies a redox reaction cycle of surface lattice oxygen, reactants, and oxygen, focusing on surface redox reactions, i.e., the source of oxygen required for toluene oxidation is lattice oxygen. Fig. 2c illustrates the linearity data fitted by the MVK model at each temperature point. The reaction rate constants derived from the slope for temperature points were then collected and plotted linearity using Arrhenius equation. As shown in Fig. 2d,

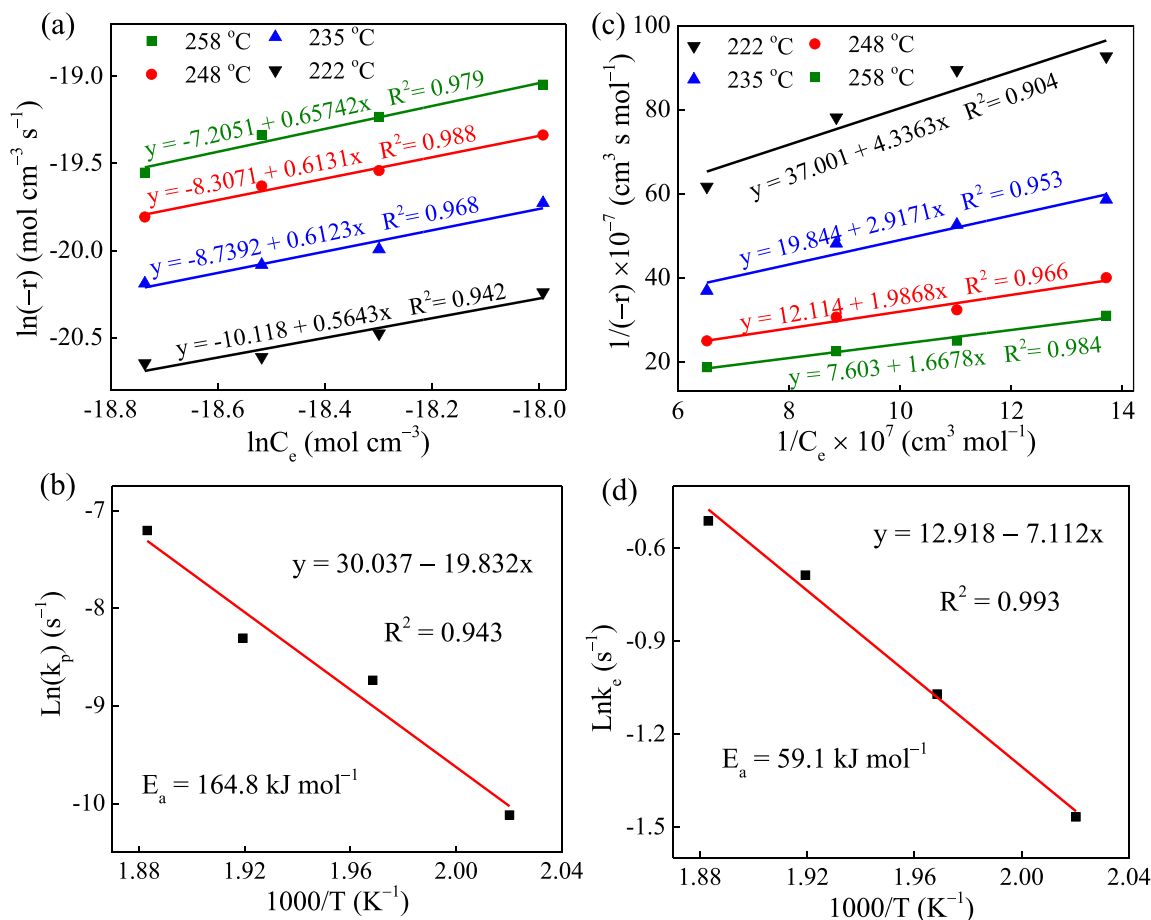


**Fig. 2.** (a) and (b) linear fitting of  $C_7H_8$  oxidation for the PL model and corresponded Arrhenius equation, respectively; (c) and (d) linear fitting of  $C_7H_8$  oxidation for the MVK model and corresponded Arrhenius equation, respectively.

the results show the  $R^2$  value is 0.993 and the activation energy  $E_a$  was obtained as 59.1 kJ/mol and frequency factor  $A$  of  $0.41 \times 10^6$  s<sup>-1</sup>. Based on chemical mechanism, the MVK consists of the two stages occurred in the catalytic reaction between the catalyst and  $C_7H_8$  (Wang et al., 2018). The first stage is the interaction of  $C_7H_8$  with the lattice oxygen on the surface of the metal oxide, resulting in the formation of  $CO_2$  and  $H_2O$ , which was proved in mass balance discussion part. The followed stage relates to the supplement of lattice oxygen by adsorbed oxygen in the gas phase for the next cycle of reactions.

### 3.2.3. Langmuir Hinshelwood model

From the result of the MVK model, the oxygen concentration is assumed to have no effect on the catalytic reactions; it can therefore be a constant. However, the L-H model shows that the oxygen concentration has a higher correlation with the catalytic reaction rate than the  $C_7H_8$  concentration. Fig. 3 illustrated the linearity curves with high  $R^2$  values fitted by L-H model. The  $K'$  and  $K''$  values for each line can be derived from the slope and intercept and shown in Table S3. Even though the  $O_2$  concentration is greater than  $C_7H_8$  concentration, its influence on the catalytic oxidation of  $C_7H_8$  should be put in a deep consideration to get more understanding of the oxidation kinetics and mechanism as well. Typically, the interaction of reactants (toluene) and  $O_2$  on the catalyst surface can be described by L-H model. If we assume that  $C_7H_8$  and  $O_2$  adsorb at the same activation position, the progress of

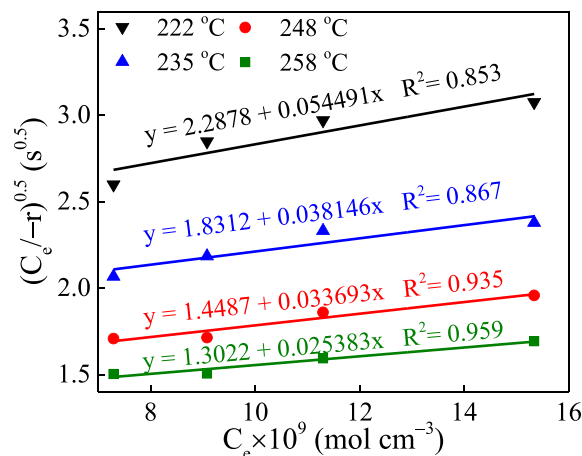


**Fig. 3.** Linear fitting of  $C_7H_8$  oxidation for the L-H model.

the catalytic reaction should then be discussed. In other words, both lattice oxygen and adsorbed oxygen participate in the  $C_7H_8$  oxidation reaction, which also agrees with previous studies (Tang et al., 2018; Gao et al., 2018). The reaction rate in the case of fixed  $C_7H_8$  concentration and altered  $O_2$  concentration is shown in Table S4.

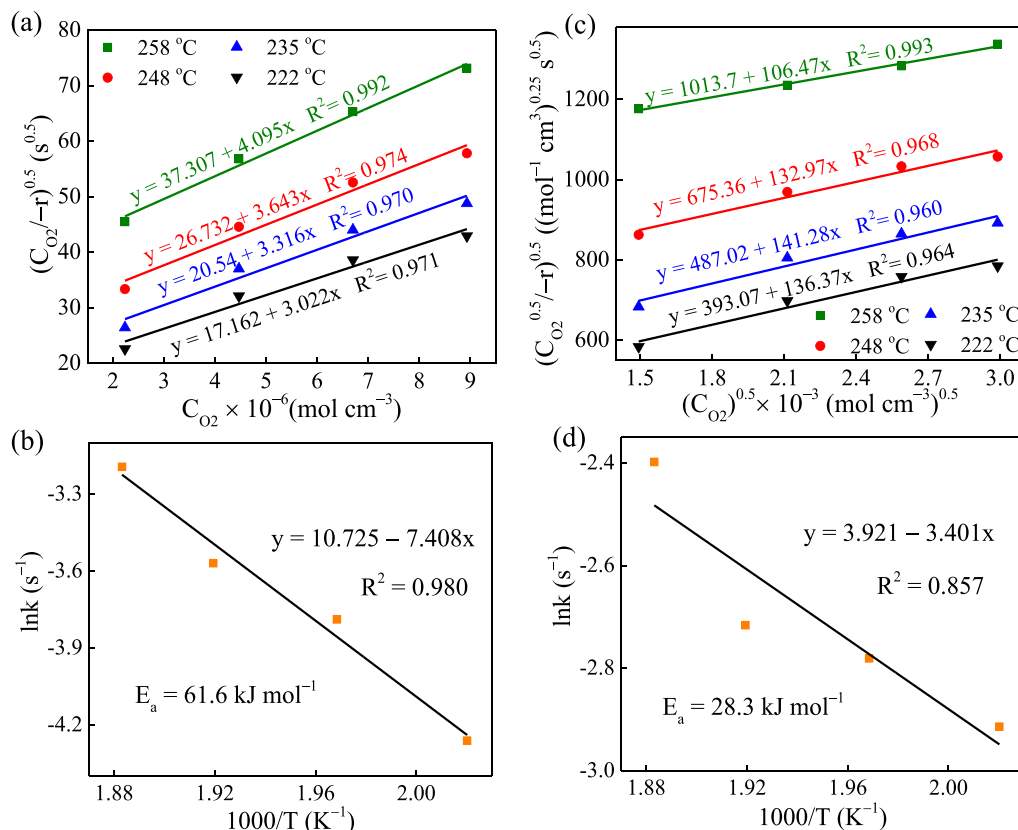


**Fig. 4.** (a) and (b) kinetic linear fitting of C<sub>7</sub>H<sub>8</sub> oxidation in the case of K<sub>1</sub>', K<sub>1</sub>'' by the L-H model and Arrhenius equation, respectively; (c) and (d) kinetic linear fitting of C<sub>7</sub>H<sub>8</sub> oxidation in the case of K<sub>2</sub>', K<sub>2</sub>'' by the L-H model and Arrhenius equation, respectively.

The result data are then substituted to Eq. (14) and plotted the linear regression at various heating temperatures (Fig. 4a) to show the dependence of reaction rate on the oxygen molecules (O<sub>2</sub>). Subsequently, K<sub>1</sub>' and K<sub>1</sub>'' at each temperature point can be derived from the intercept and slope of the linear equation (Table S5). When temperature increases, both K<sub>1</sub>' and K<sub>1</sub>'' decrease. The obtained data of K', K'', K<sub>1</sub>', and K<sub>1</sub>'' are combined with the known values of C<sub>e</sub> and C<sub>O<sub>2</sub></sub> to compute the value of k, K<sub>e</sub>, K<sub>O<sub>2</sub></sub> for the O<sub>2</sub> adsorption. Fig. 4b exhibits the rate constant k fitted by the Arrhenius plot and the obtained activation energy of 61.6 kJ mol<sup>-1</sup>, which is within the range for the catalytic reaction (Tseng and Chu, 2001). Previous studies have also proved that the adsorption of oxygen molecules on the catalyst surface is a vital step during the catalytic process of pollutants oxidation (Tseng and Chu, 2001; Chu et al., 2001).

Similarly, by substituting the achieved data to Eq. (15), a linear regression at various heating temperatures can be plotted (Fig. 4c) to show the dependence of reaction rate on the oxygen atoms (O). Herein, K<sub>2</sub>' and K<sub>2</sub>'' at each temperature point can be derived from the intercept and slope of the linear equation (Table S6). The values of K', K'', K<sub>2</sub>', and K<sub>2</sub>'' are combined with the known values of C<sub>e</sub> and C<sub>O<sub>2</sub></sub>, the value of k, K<sub>e</sub>, K<sub>O<sub>2</sub></sub> for the reaction involved with O adsorption can also be estimated from their definition. Fig. 4d exhibits the Arrhenius equation fitting of rate constant and activation energy of 28.3 kJ mol<sup>-1</sup>. In both cases, the plot for calculating K' and K'' shows that the catalytic reaction has a lower correlation with the adsorption of reactants, while K<sub>1</sub>', K<sub>1</sub>'' and K<sub>2</sub>', K<sub>2</sub>'' plotting show high linearity of the attributable oxygen concentration. Therefore, the L-H model indicates that the main influencing factors of the catalytic reaction have a low correlation with the reactant adsorption but a high correlation with the redox properties of metal oxides.

This redox ability may come from the metal itself or be affected by the desorption of the product on the surface.

### 3.3. The change of chemical compositions and states after catalytic reaction

#### 3.3.1. XANES

Fig. 5a shows that there is almost no change in the valence and structure of the spectrum of Fe before and after the reaction. Therefore, it can be inferred that Fe<sub>2</sub>O<sub>3</sub> plays a role as an electron balance, transfer, and structure stability in the catalytic reaction of the toluene oxidation process.

In Fig. 5b, the XANES spectrum of Mn reduced slightly, from 14.891 eV before the reaction to 13.996 eV after the reaction (set E<sub>0</sub> = 6542 eV), indicating that part of Mn might be reduced from Mn<sup>4+</sup> to Mn<sup>3+</sup> state (Manceau et al., 2012). This result suggests the establishment of oxygen vacancies to compensate for the charge loss. In Fig. 5c, the spectra of Cu before and after the catalytic reaction are slightly different, indicating that the structure and the valence did not change. Hence, it can be estimated that Cu may also serve as an active center, but the effect is not as good as Mn.

In summary, the XANES results show the reduction of Fe, Mn, and Cu. The activation of Mn<sup>4+</sup> was documented to be more active than noble metal oxides and gives better catalytic performance (Wu et al., 2013). It was also reported that a synergistic combination of copper and manganese provides more active sites than individual ones (Aguilera et al., 2011). Einaga et al. demonstrated the incorporation of Cu into Mn oxides can build up the average oxidation state of Mn on the surface sites higher than bulk sites, result-

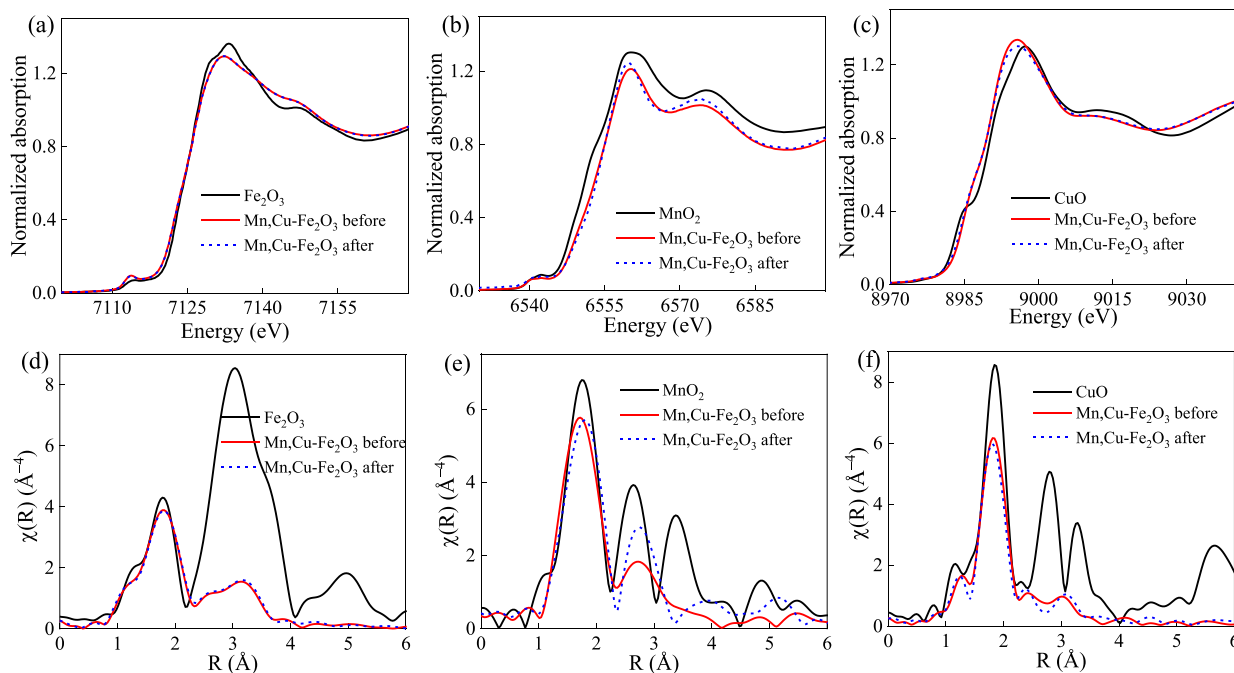


Fig. 5. XANES (a, b, c) and EXAFS (d, e, f) of Fe, Mn, and Cu before and after catalytic oxidation, respectively.

ing in higher activity compared to single-metal oxides (Einaga et al., 2014).

### 3.3.2. EXAFS

As shown in Fig. 5d, there is almost no difference in Fe structure between before and after the reaction. Therefore, it can be determined that Fe may act as an electron balance or transfer or a carrier in the catalytic reaction. The formation of Fe/CuO<sub>x</sub> composite reduces the phase shift of Mn oxide. In Mn K-edge EXAFS (Fig. 5e), the 1–2 Å Mn-O in the first layer is slightly shifted, and the second layer Mn-O-Mn has more obvious changes, indicating that Mn may be the main reaction activation center of the catalyst (Kou et al., 1998). Hence, it can be concluded that the activation center of Mn could be the formation of a complex structure from Mn<sup>3+</sup> and Mn<sup>4+</sup>. The results show that it may be part of the partial reduction process of Mn<sup>4+</sup> to Mn<sup>3+</sup>. The change in Mn-O-Mn structure of the second layer about 2–3 Å might come from the adsorption of reactants and products on the catalyst surface (Yang et al., 2020). This interference signal is generated by Mn-O-C, which superimposes with the original layer.

Accordingly, Mn-O-Mn will cause the change and compensation of the signal and become significant changes after 3 Å. The results of the EXAFS analysis of Cu in Fig. 5f show a slight change in the structure of the catalyst after the catalytic reaction. Hence, the activation center is formed by co-doping of Mn and Cu the composite structure of Mn<sup>3+</sup> and Mn<sup>4+</sup>, resulting in higher catalytic reaction activity. Therefore, the formation of part of the Mn and Cu structures in Mn,Cu-Fe<sub>2</sub>O<sub>3</sub> can also improve the reactivity. Li et al. have demonstrated the existence of Cu<sup>2+</sup>/Mn<sup>3+</sup> ↔ Cu<sup>+</sup>/Mn<sup>4+</sup> in the reaction system (Li et al., 2021). The authors also stated that in the metal oxide catalyst, the reaction is based on the redox of the metals and the interaction between the lattice O and oxygen. The effect of Cu<sup>2+</sup>/Mn<sup>3+</sup> ↔ Cu<sup>+</sup>/Mn<sup>4+</sup> can reduce the hindrance of the aforementioned reaction, resulting in the improvement of the catalytic efficiency. Besides, the mixed structure of Mn<sup>3+</sup> and Mn<sup>4+</sup> accelerates the electron transfer and speeds up the catalytic reaction.

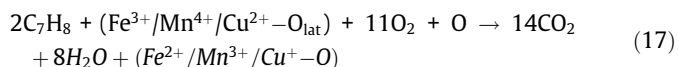
Therefore, the formation of Mn/Cu structure in Mn,Cu-Fe<sub>2</sub>O<sub>3</sub> composite can also improve the reactivity.

### 3.4. Catalytic reaction mechanism

The reaction mechanism of gas catalytic oxidation is examined and demonstrated by the hypothetical computation and analysis of the reaction kinetic models. The calculation results of the activation energy of each catalytic reaction are shown in Table S7. The P-L model represents a relationship between two quantities, in which one changes as a power other. Therefore, it is only applied for heterogeneous reactions in high-temperature condition. In this case, the calculated E<sub>a</sub> is 164.8 kJ mol<sup>-1</sup>, which is the highest compared to other models. Meanwhile, the MVK model mainly discusses the redox cycle between the C<sub>7</sub>H<sub>8</sub> and the lattice oxygen of the metal oxide surface in the catalytic reaction, forming oxygen vacancies. This theory matches the calculated E<sub>a</sub> (59.1 kJ mol<sup>-1</sup>). In contrast, based on the kinetic data that both oxygen species participate in the oxidation reaction, the L-H model demonstrates that oxygen concentration has a high correlation with the reaction rate, i.e., the reaction is also supported by O or O<sub>2</sub> binding of metal oxides on the catalyst surface. Therefore, the L-H model is appropriate for the catalytic reaction involving molecular (E<sub>a</sub> = 61.6 kJ mol<sup>-1</sup>) and atomic oxygen adsorption (E<sub>a</sub> = 28.3 kJ mol<sup>-1</sup>). The E<sub>a</sub> values calculated by MVK and O<sub>2</sub> adsorption-related L-H models are almost the same, which indicates that both models correspond to the participation of adsorbed oxygen on the catalyst surface. Therefore, it can be concluded that the calculation results in MVK and L-H models consolidate the reactions proposed in Eqs. (4), 5, 8, 9, and 10. The lowest E<sub>a</sub> obtained in the case of the O adsorption-related L-H model demonstrates that atomic oxygen is easy to be adsorbed on the catalyst surface and then triggers the oxidation reaction to happen faster, compared to molecular oxygen. In summary, the MVK model can be the most workable for the description of toluene catalytic oxidation over Mn,Cu-Fe<sub>2</sub>O<sub>3</sub> composite, whereas the L-H model could be feasible to

describe the kinetics of oxygen adsorption and oxygen-involved reaction mechanism.

Moreover, characterization analysis after the catalytic test confirms that the change of Mn,Cu-Fe<sub>2</sub>O<sub>3</sub> during the catalytic oxidation of toluene is related to the reduction of Mn,Cu-Fe<sub>2</sub>O<sub>3</sub> catalyst. Based on the results of XAS (XANES and EXAFS) analysis, combined with kinetic models, it can be inferred that the reaction process is as follows:



At lower energy, C<sub>7</sub>H<sub>8</sub> is first partially oxidized to form an intermediate product of Mn,Cu-Fe<sub>2</sub>O<sub>3</sub>-CO. Some of the electrons are transferred to Mn<sup>4+</sup> to reduce Mn<sup>4+</sup> to form Mn<sup>3+</sup>. After breaking the Mn,Cu-Fe<sub>2</sub>O<sub>3</sub> from Mn,Cu-Fe<sub>2</sub>O<sub>3</sub>-CO, the -CO bond is completely oxidized to form CO<sub>2</sub> and desorbed from the surface. Fe<sup>2+</sup>/Mn<sup>3+</sup>/Cu<sup>+</sup> reacts with oxygen and is then oxidized to Mn<sup>4+</sup>, forming a catalytic reaction cycle.

#### 4. Conclusion

A new approach to the linearity of the kinetic models for evaluating the reaction mechanism versus experimental data of toluene catalytic oxidation in a continuous-flow reactor was developed based on the consideration of reactant fluctuation. The conversion rate of toluene oxidation over Mn,Cu-Fe<sub>2</sub>O<sub>3</sub> is proportional to C<sub>7</sub>H<sub>8</sub> and O<sub>2</sub> concentration and temperature. However, the toluene conversion rate is disproportional to the flow rate due to the limit of active sites on the catalyst surface and correlative reaction between C<sub>7</sub>H<sub>8</sub> and O<sub>2</sub>. The enhancement of C<sub>7</sub>H<sub>8</sub> adsorption on the Mn,Cu-Fe<sub>2</sub>O<sub>3</sub> catalyst surface with high redox property induces the complete oxidation of C<sub>7</sub>H<sub>8</sub> to CO<sub>2</sub>. As a result, the initial concentrations of toluene of 165 ppmv and oxygen of 10% at a flow rate of 200 mL min<sup>-1</sup> give the highest catalytic performance of Mn,Cu-Fe<sub>2</sub>O<sub>3</sub>. The Mars-van Krevelen model fitting data indicate the majority of the toluene catalytic oxidation process regards the interaction between C<sub>7</sub>H<sub>8</sub> and lattice oxygen on the surface of Mn,Cu-Fe<sub>2</sub>O<sub>3</sub>. Furthermore, L-H model fitting demonstrates that adsorbed oxygen species also participated in the catalytic reactions. The surface reaction mechanism of toluene oxidation over Mn,Cu-Fe<sub>2</sub>O<sub>3</sub> catalyst was proposed through the newly developed kinetic models and surface characterization (XANES and EXAFS) of the catalyst after the reaction. Overall, the importance of our findings is the applicability of kinetic models and characterization to the direct identification of catalytic reaction mechanism of gas removal process over metal oxides-based catalysts in continuous flow catalytic systems.

#### Declaration of Competing Interest

The authors declare that they have no known competing financial interests or personal relationships that could have appeared to influence the work reported in this paper.

#### Acknowledgements

Author acknowledges the CONEX-Plus programme funded by Universidad Carlos III de Madrid (UC3M) and the European Commission through the Marie-Sklodowska Curie COFUND Action (Grant Agreement No 801538). The authors extend their sincere appreciation to the Researchers Supporting Project number (RSPD2023R682), King Saud University, Riyadh, Saudi Arabia for the support.

#### Appendix A. Supplementary material

Supplementary data to this article can be found online at <https://doi.org/10.1016/j.jksus.2023.102812>.

#### References

- Aguilera, D.A., Perez, A., Molina, R., Moreno, S., 2011. Cu-Mn and Co-Mn catalysts synthesized from hydrotalcites and their use in the oxidation of VOCs. *Appl. Catal. B-Environ.* 104, 144–150.
- Arzamendi, G., de la Peña O'Shea, V.A., Álvarez-Galván, M.C., Fierro, J.L.G., Arias, P.L., Gandía, L.M., 2009. Kinetics and selectivity of methyl-ethyl-ketone combustion in air over alumina-supported PdO<sub>x</sub>-MnO<sub>x</sub> catalysts. *J. Catal.* 261, 50–59.
- Bahlawane, N., 2006. Kinetics of methane combustion over CVD-made cobalt oxide catalysts. *Appl. Catal. B-Environ.* 67, 168–176.
- Brandt, E.M.F., Duarte, F.V., Vieira, J.P.R., Melo, V.M., Souza, C.L., Araújo, J.C., Chernicharo, C.A.L., 2016. The use of novel packing material for improving methane oxidation in biofilters. *J. Environ. Manage.* 182, 412–420.
- Cai, Z., Li, F., Rong, M., Lin, L., Yao, Q., Huang, Y., Chen, X., Wang, X., 2019. Chapter 1 - Introduction. In: Wang, X., Chen, X. (Eds.), *Novel Nanomaterials for Biomedical, Environmental and Energy Applications*. Elsevier, pp. 1–36.
- Chu, H., Hao, G.H., Tseng, T.K., 2001. The kinetics of catalytic incineration of dimethyl sulfide and dimethyl disulfide over an MnO/Fe<sub>2</sub>O<sub>3</sub> catalyst. *J. Air Waste Manag. Assoc.* 51, 574–581.
- Dang, V.D., Adorna Jr, J., Annadurai, T., Bui, T.A.N., Tran, H.L., Lin, L.-Y., Doong, R.-A., 2021. Indirect Z-scheme nitrogen-doped carbon dot decorated Bi<sub>2</sub>MoO<sub>6</sub>/g-C<sub>3</sub>N<sub>4</sub> photocatalyst for enhanced visible-light-driven degradation of ciprofloxacin. *Chem. Eng. J.* 422, 130103.
- Einaga, H., Kiya, A., Yoshioka, S., Teraoka, Y., 2014. Catalytic properties of copper-manganese mixed oxides prepared by coprecipitation using tetramethylammonium hydroxide. *Catal. Sci. Technol.* 4, 3713–3722.
- Figueredo, M.J.M., Andana, T., Bensaid, S., Dosa, M., Fino, D., Russo, N., Piumetti, M., 2020. Cerium-copper-manganese oxides synthesized via solution combustion synthesis (SCS) for total oxidation of VOCs. *Catal. Lett.* 150, 1821–1840.
- Gao, T., Chen, J., Fang, W., Cao, Q., Su, W., Dumeignil, F., 2018. Ru/Mn<sub>x</sub>Ce<sub>1-x</sub>O<sub>y</sub> catalysts with enhanced oxygen mobility and strong metal-support interaction: exceptional performances in 5-hydroxymethylfurfural base-free aerobic oxidation. *J. Catal.* 368, 53–68.
- Genty, E., Siffert, S., Cousin, R., 2019. Investigation of reaction mechanism and kinetic modelling for the toluene total oxidation in presence of CoAlCe catalyst. *Catal. Today* 333, 28–35.
- Halim, K.A., Khedr, M., Nasr, M., El-Mansy, A., 2007. Factors affecting CO oxidation over nanosized Fe<sub>2</sub>O<sub>3</sub>. *Mater. Res. Bull.* 42, 731–741.
- He, L., Fan, Y., Bellettre, J., Yue, J., Luo, L., 2020. A review on catalytic methane combustion at low temperatures: Catalysts, mechanisms, reaction conditions and reactor designs. *Renew. Sustain. Energy Rev.* 119, 109589.
- Hu, C., 2011. Catalytic combustion kinetics of acetone and toluene over Cu<sub>0.15</sub>Ce<sub>0.87</sub>O<sub>y</sub> catalyst. *Chem. Eng. J.* 168, 1185–1192.
- Kou, Y., Zhang, B., Niu, J.-Z., Li, S.-B., Wang, H.-L., Tanaka, T., Yoshida, S., 1998. Amorphous features of working catalysts: XAFS and XPS characterization of Mn/Na<sub>2</sub>WO<sub>4</sub>/SiO<sub>2</sub> as used for the oxidative coupling of methane. *J. Catal.* 173, 399–408.
- Li, G., Li, N., Sun, Y., Qu, Y., Jiang, Z., Zhao, Z., Zhang, Z., Cheng, J., Hao, Z., 2021. Efficient defect engineering in Co-Mn binary oxides for low-temperature propane oxidation. *Appl. Catal. B-Environ.* 282, 119512.
- Li, J.-R., Zhang, W.-P., Li, C., Xiao, H., He, C., 2021. Insight into the catalytic performance and reaction routes for toluene total oxidation over facilely prepared Mn-Cu bimetallic oxide catalysts. *Appl. Surf. Sci.* 550, 149179.
- Lin, L.-Y., Liu, C., Dien Dang, V., Fu, H.-T., 2023. Atomically dispersed Ti-O clusters anchored on NH<sub>2</sub>-UiO-66(Zr) as efficient and deactivation-resistant photocatalyst for abatement of gaseous toluene under visible light. *J. Colloid Interface Sci.* 635, 323–335.
- Liu, L., Sun, J., Ding, J., Zhang, Y., Jia, J., Sun, T., 2019. Catalytic oxidation of VOCs over SmMnO<sub>3</sub> perovskites: catalyst synthesis, change mechanism of active species, and degradation path of toluene. *Inorg. Chem.* 58, 14275–14283.
- Mahmood, A., Wang, X., Xie, X., Sun, J., 2021. Degradation behavior of mixed and isolated aromatic ring containing VOCs: Langmuir-Hinshelwood kinetics, photodegradation, in-situ FTIR and DFT studies. *J. Environ. Chem. Eng.* 9, 105069.
- Manceau, A., Marcus, M.A., Grangeon, S., 2012. Determination of Mn valence states in mixed-valent manganates by XANES spectroscopy. *Am. Mineral.* 97, 816–827.
- Mohammed, A.R., Adamu, U., Gideon, S., Sani, U., 2020. Computational kinetic study on atmospheric oxidation reaction mechanism of 1-fluoro-2-methoxypropane with OH and ClO radicals. *J. King Saud Univ. Sci.* 32, 587–594.
- Pandhare, N.N., Pudi, S.M., Mondal, S., Pareta, K., Kumar, M., Biswas, P., 2018. Development of kinetic model for hydrogenolysis of glycerol over Cu/MgO catalyst in a slurry reactor. *Ind. Eng. Chem. Res.* 57, 101–110.
- Shakor, Z.M., Ramos, M.J., AbdulRazak, A.A., 2022. A detailed reaction kinetic model of light naphtha isomerization on Pt/zeolite catalyst. *J. King Saud Univ. - Eng. Sci.* 34, 303–308.
- Su, Z., Yang, W., Wang, C., Xiong, S., Cao, X., Peng, Y., Si, W., Weng, Y., Xue, M., Li, J., 2020. Roles of oxygen vacancies in the bulk and surface of CeO<sub>2</sub> for toluene catalytic combustion. *Environ. Sci. Technol.* 54, 12684–12692.

- Tang, M., Liu, K., Roddick, D.M., Fan, M., 2018. Enhanced lattice oxygen reactivity over  $\text{Fe}_2\text{O}_3/\text{Al}_2\text{O}_3$  redox catalyst for chemical-looping dry ( $\text{CO}_2$ ) reforming of  $\text{CH}_4$ : Synergistic La-Ce effect. *J. Catal.* 368, 38–52.
- Teo, B.K., 2012. EXAFS: Basic Principles and Data Analysis. Springer Science & Business Media.
- Tseng, T.-K., Chu, H., 2001. The kinetics of catalytic incineration of styrene over a  $\text{MnO}/\text{Fe}_2\text{O}_3$  catalyst. *Sci. Total Environ.* 275, 83–93.
- Vannice, M.A., 2007. An analysis of the Mars–van Krevelen rate expression. *Catal. Today* 123, 18–22.
- Wang, C.-H., Lin, S.-S., Weng, H.-S., 2002. The kinetics of catalytic incineration of  $(\text{CH}_3)_2\text{S}_2$  over the  $\text{CuO}-\text{MoO}_3/\gamma-\text{Al}_2\text{O}_3$  catalyst. *J. Environ. Sci. Health A* 37, 1649–1663.
- Wang, H., Luo, S., Zhang, M., Liu, W., Wu, X., Liu, S., 2018. Roles of oxygen vacancy and  $\text{O}_x^-$  in oxidation reactions over  $\text{CeO}_2$  and  $\text{Ag}/\text{CeO}_2$  nanorod model catalysts. *J. Catal.* 368, 365–378.
- Wu, Y., Lu, Y., Song, C., Ma, Z., Xing, S., Gao, Y., 2013. A novel redox-precipitation method for the preparation of  $\alpha-\text{MnO}_2$  with a high surface  $\text{Mn}^{4+}$  concentration and its activity toward complete catalytic oxidation of o-xylene. *Catal. Today* 201, 32–39.
- Wu, Y., Chen, A., Liu, X., Xu, J., Wang, Y., Mumford, K., Stevens, G.W., Fei, W., 2021. Kinetic study of highly efficient  $\text{CO}_2$  fixation into propylene carbonate using a continuous-flow reactor. *Chem. Eng. Process.: Process Intensif.* 159, 108235.
- Xu, P., Ding, C., Li, Z., Yu, R., Cui, H., Gao, S., 2023. Photocatalytic degradation of air pollutant by modified nano titanium oxide ( $\text{TiO}_2$ ) in a fluidized bed photoreactor: Optimizing and kinetic modeling. *Chemosphere* 319, 137995.
- Yang, J., Zeng, D., Zhang, Q., Cui, R., Hassan, M., Dong, L., Li, J., He, Y., 2020. Single Mn atom anchored on N-doped porous carbon as highly efficient Fenton-like catalyst for the degradation of organic contaminants. *Appl. Catal. B-Environ.* 279, 119363.
- Zang, M., Zhao, C., Wang, Y., Chen, S., 2019. A review of recent advances in catalytic combustion of VOCs on perovskite-type catalysts. *J. Saudi Chem. Soc.* 23, 645–654.
- Zhang, Z.-F., Zhang, X., Zhang, X.-M., Liu, L.-Y., Li, Y.-F., Sun, W., 2020. Indoor occurrence and health risk of formaldehyde, toluene, xylene and total volatile organic compounds derived from an extensive monitoring campaign in Harbin, a megacity of China. *Chemosphere* 250, 126324.
- Zhao, Z., Miller, J.T., Wu, T., Schweitzer, N.M., Wong, M.S., 2015. EXAFS characterization of palladium-on-gold catalysts before and after glycerol oxidation. *Top. Catal.* 58, 302–313.
- Zhao, Z., Cao, Y., Dong, F., Wu, F., Li, B., Zhang, Q., Zhou, Y., 2019. The activation of oxygen through oxygen vacancies in  $\text{BiOCl}/\text{PPy}$  to inhibit toxic intermediates and enhance the activity of photocatalytic nitric oxide removal. *Nanoscale* 11, 6360–6367.
- Zou, W., Gao, B., Ok, Y.S., Dong, L., 2019. Integrated adsorption and photocatalytic degradation of volatile organic compounds (VOCs) using carbon-based nanocomposites: a critical review. *Chemosphere* 218, 845–859.